UKAEA-CCFE-PR(23)162

E. Parr, K. G. McClements, W. W. Heidbrink, C. Michael, G. Prechel, J. Rivero-Rodriguez

Studying fast-ion populations using ssNPA-signal and NBI-power oscillations

Studying fast-ion populations using ssNPA-signal and NBI-power oscillations

E. Parr, K. G. McClements, W. W. Heidbrink, C. Michael, G. Prechel, J. Rivero-Rodriguez

This is a preprint of a paper submitted for publication in Review of Scientific Instruments

Studying fast-ion populations using ssNPA-signal and NBI-power oscillations

E. Parr,[1] K. G. McClements,[1] W. W. Heidbrink,[2]
C. Michael,[3] G. Prechel,[2] and J. Rivero-Rodriguez[1]

[1] *UKAEA, Culham Science Centre, Oxfordshire OX14 3DB, UK*

[2] *University of California Irvine, Irvine CA 92697, USA*

[3] *University of California, Los Angeles, CA 90095, USA*

(Dated: September 22, 2023)

Abstract

A method for determining the fast-ion population density in magnetically-confined plasmas as a function of radius-pitch values, (R, λ), using ssNPA-signal and NBI power-output data has been developed. Oscillations in the NBI power output are replicated only in the *active* part of the ssNPA signal, allowing this to be separated from the *passive* and background signals which usually complicate data from this diagnostic. Results obtained using this method are compared with those from standard techniques using data from the MAST-U spherical tokamak.

I. INTRODUCTION

Fast-ion (FI) populations in magnetically-confined plasmas are key to plasma heating and, in the case of fast ions introduced through neutral beams, plasma current drive as well. Redistribution and loss of these fast ions, however, may be caused by instabilities in the plasma, many of which are driven by the fast ions themselves. It is therefore vital to understand the distribution and evolution of these populations in order to produce high-performance magnetically-confined fusion plasmas.

One type of diagnostic which is used in the study of fast ions is the solid-state neutral-particle analyser (ssNPA) [1–7]. These devices measure fast-ion populations via the fast-neutral (FN) fluxes produced following charge-exchange (CX) with neutrals (e.g. in deuterium plasmas: $\mathrm{D}^{+}_{\mathrm{FI}} + \mathrm{D}^{0} \rightarrow \mathrm{D}^{0}_{\mathrm{FN}} + \mathrm{D}^{+}$). As CX involves negligible momentum transfer, and the fast neutrals subsequently escape the plasma unperturbed in straight-line trajectories, all of the velocity information of the preceding fast ion is preserved. As an *active* diagnostic, the ssNPA relies on neutrals from neutral-beam injection (NBI) heating systems to induce CX. Compact silicon photo-diodes used in ssNPA diagnostics allow multiple lines-of-sight to be established, intersecting the neutral beam at varying plasma major radii, R, and pitch, λ (ratio of the ion velocity parallel to, and in the direction of, the magnetic field, $v_{||}$, and the total, v_{total}). Considering the fast-ion population density distribution in velocity space co-ordinates, $f_{\mathrm{FI}}(R,\, z,\, \lambda,\, E,\, t)$, ssNPA diagnostics allow for a particular slice of this distribution – with respect to $(R,\, \lambda)$ – to be measured. Here z is the vertical spacial co-ordinate, defined with respect to the plane in-which the lines-of-sight lie (normally this is the geometric mid-plane of the device). Use of the ssNPA in current mode [3, 4, 6, 7] produces a voltage output, S, which is, in principle, proportional to the rate of the incoming fast-neutral flux, irrespective of energy, E. The portion of the fast-ion energy distribution which may be measured by the ssNPA in current mode is therefore an integral over the transmission efficiency, ϵ_{n}, for neutrals in the detector,

$$N_{\mathrm{FI}} = \int \epsilon_{\mathrm{n}}(E) \cdot f_{\mathrm{FI}}(E) \cdot dE. \tag{1}$$

Here the detector efficiency effectively gives a threshold energy for fast-ion measurement, which is determined by the material and thickness of the filter used. The use of different filter thicknesses for detectors with the same line-of-sight can also be used to offer some information on the fast-ion energy distribution. The loss in energy-spectroscopy capabilities of current mode is countered by excellent time resolution. In the Mega-Amp Spherical Tokamak Upgrade (MAST-U) fast-ion populations have been studied using ssNPA data at 2 μs intervals [7]. This is particularly useful in the study of fast-ion redistribution and loss following instabilities that occur on relatively short time-scales, such as sawteeth.

One issue, however, with using active diagnostics such as the ssNPA is that the neutrals which induce CX in fast ions are not only provided by the NBI but are present as a background minority species in the plasma. The signal produced from CX between fast ions and these background neutrals, the so-called *passive* signal (S_{p}), is then measured together with the desired *active* signal, produced from CX with NBI neutrals (S_{a}). This can greatly complicate ssNPA results, as the fast-ion population densities producing signal are no longer only those of the $N_{\mathrm{FI}}(R,\ \lambda)$ slice at the points of line-of-sight and NBI intersection. One solution to the problem of separating these signal components is the use of a second diagnostic performing a passive measurement, toroidally-displaced from the first for which the line-of-sight does not intersect the NBI [4, 8]. The magnitude of the passive signal may then be estimated and subtracted from the total to give just the active contribution, assuming toroidal symmetry in the background neutral density. This method, however, introduces additional uncertainties into the measurements and can be complicated by different sources of background signal in the diagnostic lines-of-sight. Another method utilises *beam notching*, whereby the NBI is switched off for short periods at set intervals during the pulse. The passive and background signal component may then be ascertained in the absence of the beam and subtracted from the total signal immediately preceding the switch-off to determine the active component. However, the timing of the beam notches must be pre-set and, in MAST-U, have a minimum duration of $\sim$10 ms. It is therefore not a suitable method for studying the redistribution and loss of fast ions following instabilities, which are often unpredictable and short-lived. Also, the NBI populates the fast-ion distribution, which drives many of the instabilities. The periodic switch-off of the beam will inevitably, therefore, affect the nature and frequency of the very events that are intended to be studied.

One alternative solution to separating the active and passive signals measured with ssNPA diagnostics, which will be presently described, is to utilise oscillations in the power output of the NBI. These oscillations are replicated only in the active part of the ssNPA signal, which is proportional to both the NBI power output – proportional to the density of neutrals provided by the NBI at a given time, assuming a constant acceleration voltage – and the fast-ion density at the point of NBI and ssNPA line-of-sight intersection. The amplitude of the oscillations produced in an ssNPA signal relative to those of the NBI power output are therefore indicative of the fast-ion population density, $N_{\mathrm{FI}}(R,\, \lambda)$.

II. ANALYSIS METHOD

The active part of the ssNPA signal in current mode, S_{a}, may be expressed as,

$$S_{\mathrm{a}} = A \cdot \Sigma_{\mathrm{CX}} \cdot N_{\mathrm{NBI}} \cdot N_{\mathrm{FI}}, \tag{2}$$

where N_{NBI} is the neutral density provided by the NBI and N_{FI} is the fast-ion population density with $(R,\, \lambda)$, both at the point of line-of-sight and NBI intersection, Σ_{CX} is a coefficient containing the integrated CX cross-sections for the fast-ion energy distribution, and A embodies the overall response of the system. If an oscillation is applied to the NBI power output, δP_{NBI}, driven by changes to the beam current, each of the terms in Eq. 2 may then be expressed as the sum of a time-averaged component, e.g. $\bar{S}_{\mathrm{a}}$, and an oscillatory component, δS_{a}. For small power-output modulations the second-order oscillatory terms, as well as those associated with the A and Σ_{CX} terms, may be neglected, giving,

$$S_{\mathrm{a}} = \bar{S}_{\mathrm{a}} + \delta S_{\mathrm{a}} = A \cdot \Sigma_{\mathrm{CX}} \cdot (\bar{N}_{\mathrm{NBI}} \bar{N}_{\mathrm{FI}} + \bar{N}_{\mathrm{FI}} \delta N_{\mathrm{NBI}} + \bar{N}_{\mathrm{NBI}} \delta N_{\mathrm{FI}}), \tag{3}$$

and when considering only the oscillating part of the active signal,

$$\delta S_{\mathrm{a}} = A \cdot \Sigma_{\mathrm{CX}} \cdot (\bar{N}_{\mathrm{FI}} \delta N_{\mathrm{NBI}} + \bar{N}_{\mathrm{NBI}} \delta N_{\mathrm{FI}}). \tag{4}$$

Considering the $\bar{N}_{\mathrm{NBI}} \delta N_{\mathrm{FI}}$ term, this represents the oscillatory contribution from modulations in the fast-ion population driven by those of the NBI power output. Assuming that the slowing-down time scales for the portion of the fast-ion population being measured are considerably longer than those of the NBI power-output oscillations, then the $\bar{N}_{\mathrm{NBI}} \delta N_{\mathrm{FI}}$ term may be neglected. Assuming Σ_{CX} and A remain constant and no oscillations are present in the passive or background signal components then the fast-ion population density may be given (in suitably rescaled units) by the rate of change of S with respect to N_{NBI},

$$N_{\mathrm{FI}} = \frac{\delta S}{\delta N_{\mathrm{NBI}}}. \tag{5}$$

Some of the assumptions made above are, to some extent, borne out by data from MAST-U. Figure 1(a) shows oscillations which occur in the power output of the South-South (SS)

NBI, with Panel (b) showing a corresponding ssNPA signal output, S. It should be noted that the oscillations in the NBI power output derive almost entirely from fluctuations in the NBI current; the voltage over which the neutrals are accelerated being stable to $\sim \pm 0.5\%$. The NBI(SS) beam intersects the ssNPA lines-of-sight at the mid-plane of MAST-U, producing active signal. Here, the NBI(SS) power oscillations are clearly imprinted in the ssNPA signal as expected. This may then be compared with equivalent data from the South-West (SW) NBI in MAST-U – which has a beam trajectory above the machine mid-plane, and therefore does not intersect the ssNPA lines-of-sight – shown in Fig. 2 (a), with ssNPA data in Panel (b). The ssNPA signals measured during NBI(SW) heating [without NBI(SS)] are produced by passive contributions and background only, the latter mainly deriving from x rays with photon energy $E_\gamma \gtrsim 1.5$ keV [6]. As no oscillations in this case are observed in S we may assume that the beam modulations are replicated only in the active signal; i.e. $\delta S = \delta S_\mathrm{a}$. Furthermore, as a non-zero δN_FI term would be expected to produce oscillations in the passive signal, which are not observed, its neglect in Eq. 5 also appears justified. This gives confidence in the assumption that the oscillations in S derive directly, and solely, from those of the NBI-produced neutral density, without a contribution from fluctuations in the fast-ion density population or any other term in Eq. 2.

As the N_FI which determines the passive signal is predominently that which exists at the edge of the plasma, it is also important to investigate the possible presece of a δN_FI term across the whole plasma profile. For this, fast-ion diagnostics in which the signal is dependent only on the fast-ion density, and not the neutral density, may be used. Two such disgnostics at MAST-U are the Fission Chamber [9] and the Neutron Camera [10], which measure the neutron rates produced following D-D fusion reactions. These rates are a proxy for fast-ion densities and are measured globally or from collimated line-integrations, respectively. The observed absence of any oscillations in the signals from either of these diagnostics during SS or SW NBI heating is consistent with fast-ion populations across the whole of the plasma that do not fluctuate with δP_NBI.

Using this framework of assumptions, a method to measure the fast-ion population density from ssNPA-signal and NBI power-output data may be devised. For measured ssNPA data the total signal, S, can be separated into a time-averaged total component, $\bar{S}$, resulting from active, passive, and background signal, and an oscillatory component present only in the

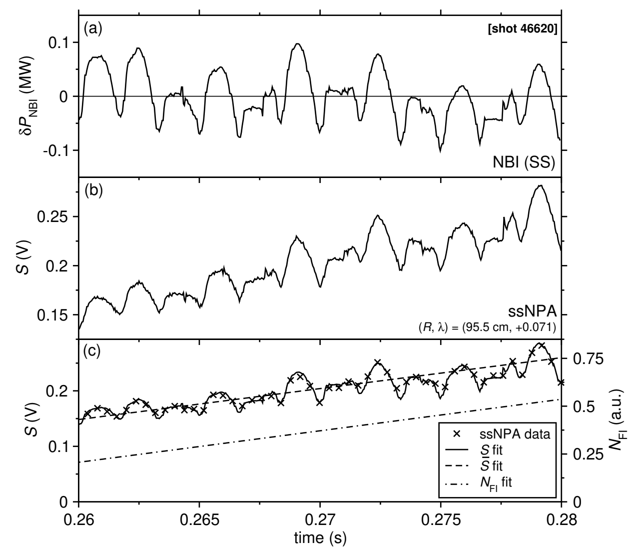

FIG. 1: Time traces from MAST-U shot number 46620. Panel (a) shows the NBI(SS) power-output oscillations, δP_{NBI}, and Panel (b) the ssNPA signal, S, from the line-of-sight intersection with NBI(SS) at $(R,\, \lambda) = (95.5$ cm, $+0.071)$. Panel (c) shows the same ssNPA data – represented as crosses, giving one in ten data points – along with the results of the fit to Eq. 7: the total fitted function, $S(t,\, \delta N_{\mathrm{NBI}})$, shown as a solid line; the smoothly-varying time-averaged rate, $\bar{S}(t)$, shown as a dashed line; the fast-ion population density, $N_{\mathrm{FI}}(t)$, shown as a dot-dashed line. The latter two variables were fitted as linear functions with respect to time.

active part of the signal,

$$S(t) = \bar{S}(t) + \delta S_{\mathrm{a}}(t). \tag{6}$$

These oscillations, δS_{a}, may be given as those of the NBI neutral density, δN_{NBI}, scaled to N_{FI}, as in Eq. 5,

$$S(t, \delta N_{\mathrm{NBI}}) = \bar{S}(t) + [N_{\mathrm{FI}}(t) \cdot \delta N_{\mathrm{NBI}}]. \tag{7}$$

The neutral-density oscillations may be given as those of the NBI power output scaled by a factor, $C(x,\, y)$, which corrects for beam intensity losses along the beam line in the toroidal x-y plane using Thomson-Scattering data of the electron-density profile, n_{n}, and the width of beam subtended by each line-of-sight,

$$\delta N_{NBI} = C(x, y) \cdot \delta P_{NBI}. \tag{8}$$

When fitting ssNPA data using Eq. 7 the oscillations of the neutral density, δN_{NBI}, represent a second independent variable, and appropriate functions with respect to time should be used

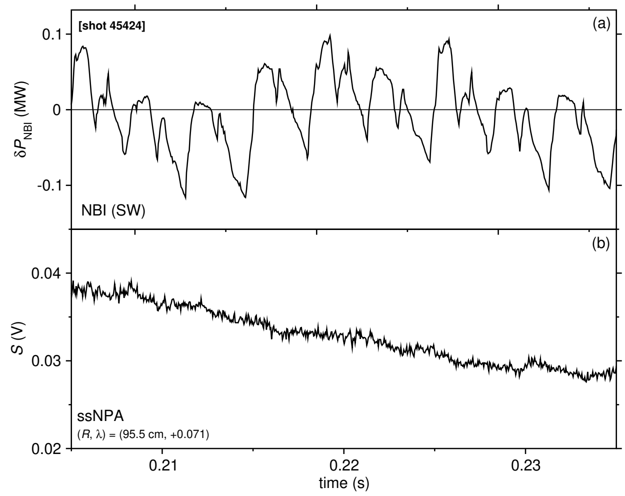

FIG. 2: Time traces from MAST-U shot number 45424. Panel (a) shows the NBI(SW) power-output oscillations, $\delta P_{\rm NBI}$, and Panel (b) the ssNPA rate, S, from the detector which would have line-of-sight intersection with NBI(SS) at (R, λ) = (95.5 cm, +0.071).

for $\bar{S}(t)$ and $N_{\rm FI}(t)$.

III. APPLICATION OF METHOD

The ssNPA on MAST-U [7] consists of three arrays, each with a tungsten filter of different thickness (100, 200, and 300 nm). Each array then consists of 15 silicon photodiode detectors, providing 15 separate lines-of-sight. These three arrays transmit neutrals with an efficiency distribution that reaches 50% (indicating the rough threshold energy) at $E \simeq 18$, 38, and 58 keV, respectively, as calculated using the SRIM software for ion energy loss in materials [11]. The same lines-of-sight and NBI(SS) interaction points are replicated in each of the three arrays, intended to provide information on the fast-ion population energy distribution. The data used for the results presented throughout this publication derive only from the array with a filter thickness of 100 nm.

The present method was applied to NBI power-output and ssNPA data taken from MAST-U shot 46620 between 260 and 280 ms [shown in Fig. 1(a) and (b), the latter for (R, λ) = (95.5 cm, +0.071), respectively]. Results were obtained by fitting the data using Eq. 7, where $\bar{S}(t)$ and $N_{\rm FI}(t)$ varied linearly with time; the results of the fit are given in Fig. 1(c). Figure 3 shows the resulting fast-ion population densities, $N_{\rm FI}(R, \lambda)$, taken at shot times t = 260 and 280 ms; the R positions of the magnetic axes at these times are also indicated.

As the NBI heats the plasma (beginning at t = 250 ms) the results illustrate how the fast-ion distribution is populated over these 20 ms, with the largest absolute, and proportional, increases around the plasma core. This may be seen in the increasing amplitude of the ssNPA signal oscillations, relative to those of the NBI(SS) power output, in Fig. 1. The proportional changes in N_{FI} over this time period do not correspond to the respective increases in S values. This is due to the latter including unknown contributions of passive and background signal.

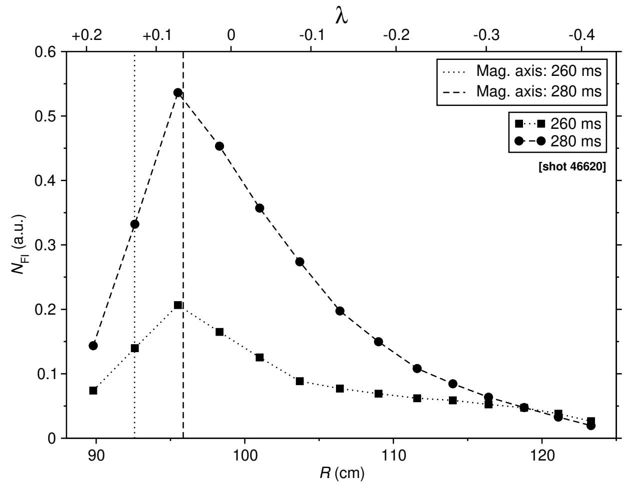

FIG. 3: Fast-ion population densities, N_{FI}, as a function of major axis, R, and pitch, λ, determined using the method presently described from ssNPA-signal and NBI(SS) power-output data. Results taken from MAST-U shot 46620 and shown for times t = 260 and 280 ms. The positions of the magnetic axes along the major axis at the times when the fast-ion populations were determined are also indicated.

A. Comparison with *beam-notching* method

The present method for determining N_{FI} may be compared with the more established *beam-notching* technique [7]. In this method the combined passive and background contributions to the ssNPA signal, $S_{\mathrm{p+bkr.}}$, for an NBI-heated plasma is determined by switching off the NBI for short periods, or notches, removing the active signal. The signal measured during this switch-off then consists of only passive and background contributions, and may be subtracted from the total signal, S, immediately preceding switch-off to estimate the active part alone. The fast-ion population density determined using the beam-notching method may be given as,

$$N'_{\text{FI}} = (S - S_{\text{p+bkr.}})/\bar{N}_{\text{NBI}}, \tag{9}$$

where $\bar{N}_{\text{NBI}}$ is the NBI neutral density [found from P_{NBI} using the $C(x, y)$ correction coefficients of Eq. 8] averaged for the time period over which S is measured. This neutral-density correction is applied to compensate for variations in P_{NBI} over both long time periods and short-term oscillations. Here, again, the CX cross-section coefficient, Σ_{CX}, is assumed to remain constant.

Figure 4 shows time traces from MAST-U shot 46620 where the beam-notching technique has been applied. The NBI(SS) power-output time-trace [Panel (a)] shows four notches of 12 ms at $t = 140$, 190, 240, and 290 ms, preceding each of which N'_{FI} may be determined. The ssNPA-signal traces for active-CX radii-pitch $(R, \lambda) =$ (92.6 cm, +0.129), (103.7 cm, -0.087), and (116.4 cm, -0.303) are shown in Panels (b-d), with the times at which the active signal may be determined indicated as (i-v) on the lower panel; the final beam-off time ($t = 596$ ms) is also highlighted, as the active signal may be determined here in the same way. As discussed, the passive ssNPA signal derives from the CX of fast ions with background neutrals in the plasma. These background neutrals are heavily concentrated at the separatrix, causing the passive signal to be essentially a measure of the pitch distribution of fast ions at the plasma edge. The mid-plane separatrix is measured to be at $R_{separatrix}$ = 130-140 cm throughout the beam-notching periods of the shot, giving pitch values measured by the passive signal of λ_{p} = +0.09, -0.07, and -0.26 for the traces in Panels (b-d), respectively.

Figure 5(a) compares results of fast-ion population densities found using the present method, N_{FI} (a), and the beam-notching method, N'_{FI} (b), for the five beam-off points in the shot. Panel (c) gives the ratio between the population densities found using these methods. Both N_{FI} and N'_{FI} values were determined using the same 2.2 ms ranges of S data, taken immediately preceding the beam-off times. Fits for $\bar{S}$ changing linearly, and N_{FI} remaining constant, as functions of time were applied. For N'_{FI}, values of $S_{p+bkr.}$ were estimated using 600 μs ranges of S data following beam-off. $S_{\text{p+bkr.}}$ signals were fitted linearly with time and values taken at the point of beam-off.

Comparing these results, the overall characteristic of the N_{FI} and N'_{FI} distributions are similar. However, a gradual reduction in N'_{FI} relative to N_{FI} is observed with increasing

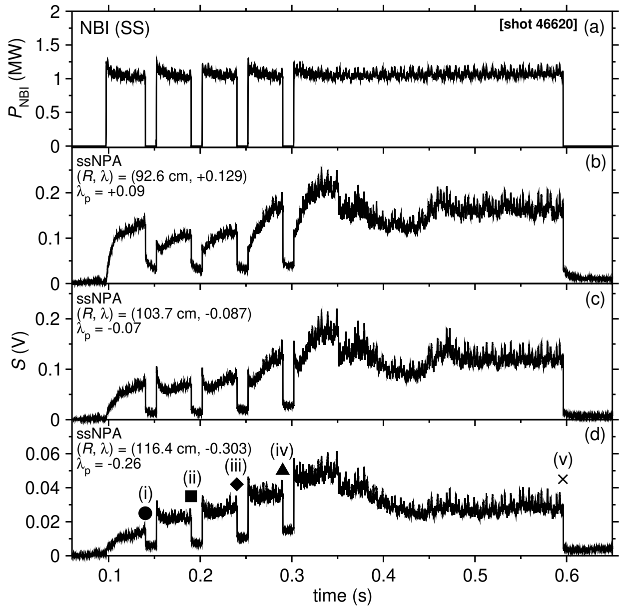

FIG. 4: Time traces from MAST-U shot 46620. Panel (a) shows the NBI(SS) power output and Panels (b-d) the ssNPA rates, S, from the line-of-sight intersections with NBI at (R, λ) = (92.6 cm, +0.129), (103.7 cm, -0.087), and (116.4 cm, -0.303) and approximate passive pitch $\lambda_{\rm p}$ = +0.09, -0.07, and -0.26 at $R_{separatrix} \sim$ 130-140 cm, respectively. The times at which $N_{\rm FI}$ and $N'_{\rm FI}$ have been calculated are indicated in Panel (d) with the corresponding symbols used in Fig. 5, and labelled (i-v).

R. This is thought to be due to non-linearity of the ssNPA output signal at low fast-neutral flux rates. The $N_{\rm FI}$ values are determined from δS measurements, which are taken over smaller voltage ranges than the S-$S_{\rm p+bkr.}$ measurements used for $N'_{\rm FI}$. Non-linearity at lower voltages could therefore lead to lower measured values of $N'_{\rm FI}$ compared with $N_{\rm FI}$; a discrepancy which would, in this case, increase with R, as the output voltages being measured reduce. The present method appears, therefore, to mitigate the effects of any non-linearity in S measurements using ssNPA diagnostics in current mode. Also, the effect of any off-set in S and $P_{\rm NBI}$ outputs is removed in the $N_{\rm FI}$ measurements; off-sets in the latter contributing to shifts between the $N'_{\rm FI}/N_{\rm FI}$ distributions of values taken at different times.

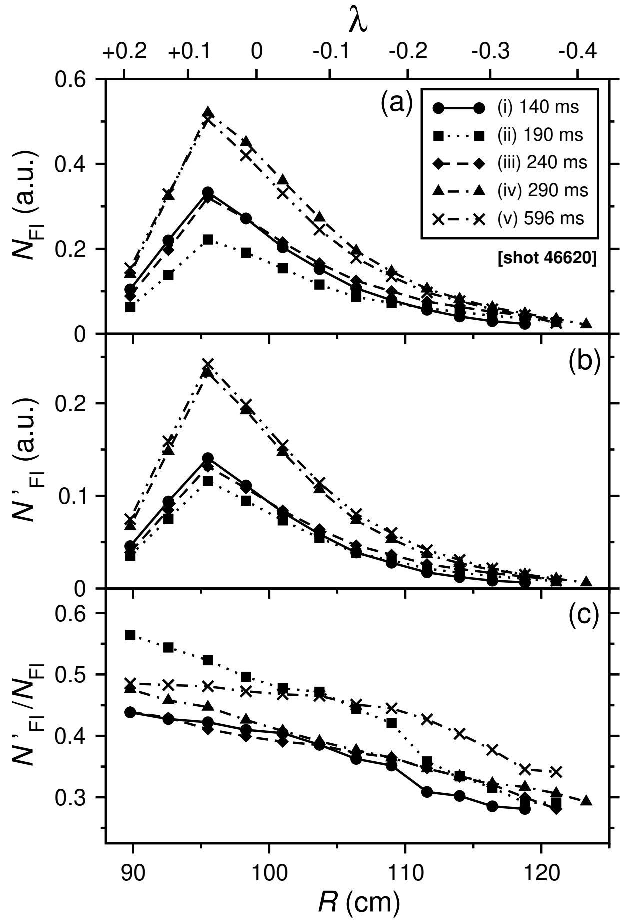

FIG. 5: Comparison of N_{FI} (a) and N'_{FI} (b) values as a function of (R, λ) using the present, and the beam-notching, methods, respectively, for data from MAST-U shot 46620 at times 140, 190, 240, 290, and 596 ms. Comparisons are made between the two sets of results in Panel (c), which gives the ratios of the values, $N'_{\mathrm{FI}}/N_{\mathrm{FI}}$.

B. Changes in fast-ion population densities following plasma events

In order to understand how the fast-ion population is affected by plasma instabilities, and how these populations may also influence instabilities, the measurement of N_{FI} prior to, and following, these events is invaluable. In this respect the beam-notching method is of little use, owing to the unpredictable nature of instabilities and the relatively long time scales in which the NBI notch must be implemented to measure what are, often, short-lived phenomena. Application of the present method, by contrast, allows for the fast-ion population to be measured throughout the time in which the active-signal inducing NBI is heating the plasma. N_{FI} may therefore be measured immediately before and after instability events, with the relative change given as,

$$\Delta N_{\text{FI}} = \frac{N_{\text{FI}}(post) - N_{\text{FI}}(pre)}{N_{\text{FI}}(pre)}. \tag{10}$$

Here *pre* and *post* refer to the fast-ion population densities before and after an event. Conventionally, changes in fast-ion populations following instability events have been studied using the total ssNPA signal, S [12]. The relative changes to this, ΔS, can then be calculated as in Eq. 10, using total S values instead of N_{FI}.

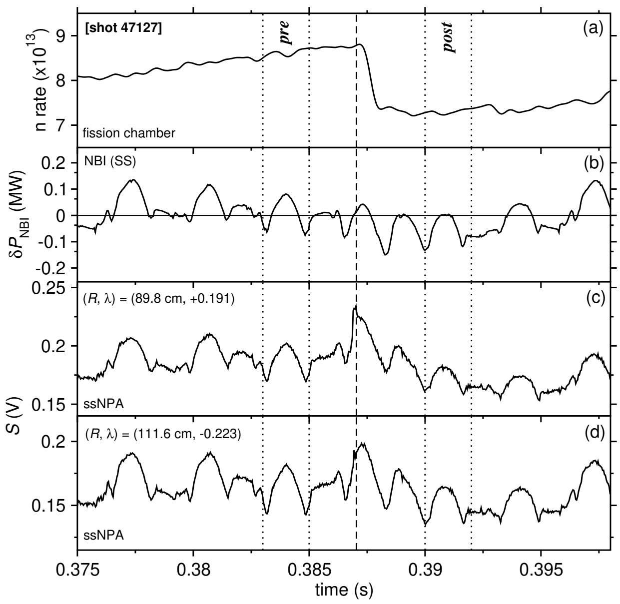

FIG. 6: Time traces indicative of a sawtooth event from MAST-U shot number 47127 as a function of shot time. Panel (a) shows the neutron rate measured by the fission chamber. Panel (b) shows the NBI(SS) power-output oscillations, δP_{NBI}, and Panels (c) and (d) show the ssNPA signal, S, from the line-of-sight intersection with NBI at (R, λ) = (89.8 cm, +0.191) and (111.6 cm, -0.223), respectively. The vertical dashed lines indicate the approximate time of the identified sawtooth event, as observed in the ssNPA time-traces, and the vertical dotted lines show the labelled ranges, pre- and post-event, over which the S and N_{FI} values were calculated using ssNPA and NBI(SS) data.

Figure 6 shows time traces corresponding to a sawtooth event identified in MAST-U shot 47127. Sawteeth are characterised by dramatic crashes in temperature and fast-ion population at the plasma core, as flux surfaces in that region with safety factor $q \leq 1$ undergo magnetic reconnection. A sharp reduction in the overall neutron rate – produced following the D-D fusion reaction – is also typically associated with sawteeth. This is illustrated in Fig. 6(a), which shows the neutron rates measured in the Fission-Chamber diagnostic. The NBI(SS) power-output oscillations are shown in Panel (b), and Panels (c) and (d) show the ssNPA signal, S, at (R, λ) = (89.8 cm, +0.191) and (111.6 cm, -0.223), respectively. The approximate time of the sawtooth event, as measured in the ssNPA signals, is indicated by the vertical dashed line. Figure 7 shows $N_{\rm FI}$ (a) and S (b) values calculated as a function of major plasma radius, R, and pitch, λ, both prior to, and following, the sawtooth event shown in Fig. 6. The relative changes to these respective quantities are then given in Panel (c). The pre- and post-sawtooth time ranges over which the data were taken for both $N_{\rm FI}$ and S value measurements are shown in Fig. 6 as dotted vertical lines.

As fast ions are ejected from the core of the plasma during sawteeth, a reduction in the active ssNPA signal would be expected across this region. Their redistribution to the plasma edge will also then lead to an expected increase in passive signal for all lines-of-sight, as they interact with the background neutrals concentrated close to the separatrix (mid-plane $R_{separatrix}$ = 137.9 cm at t = 387 ms for shot 47127). This is borne out by the present results, which show ΔS shifted above $\Delta N_{\rm FI}$ across all (R, λ) values. This is due to S including both active and passive contributions to the signal, whereas $N_{\rm FI}$ is a measures of the active only.

The utility of the present method is well illustrated in the analysis of the ssNPA time traces of Fig. 6. Oscillations in the signal complicate ΔS measurements, and correcting for $\delta P_{\rm NBI}$ is not possible as the relative proportions of active, and passive and background signal are not known. Additionally, the countering increase in passive signal make changes in S difficult to discern [notable in Panel (d), (R, λ) = (111.6 cm, -0.223)]. Conversely, changes in $N_{\rm FI}$ are clearly observed through the reduction in amplitude of oscillations of the ssNPA signal between the two ranges, pre and post event, relative to those of the NBI(SS).

IV. FUTURE WORK AND SUMMARY

The present method of analysis is applicable also to data from other active diagnostics [such as the Fast-Ion D_α (FIDA) diagnostic [8]] to determine fast-ion distributions as a function of R along the intersecting beam line. Further refinement of the technique may also be provided by using oscillations in the neutral density along the beam line which

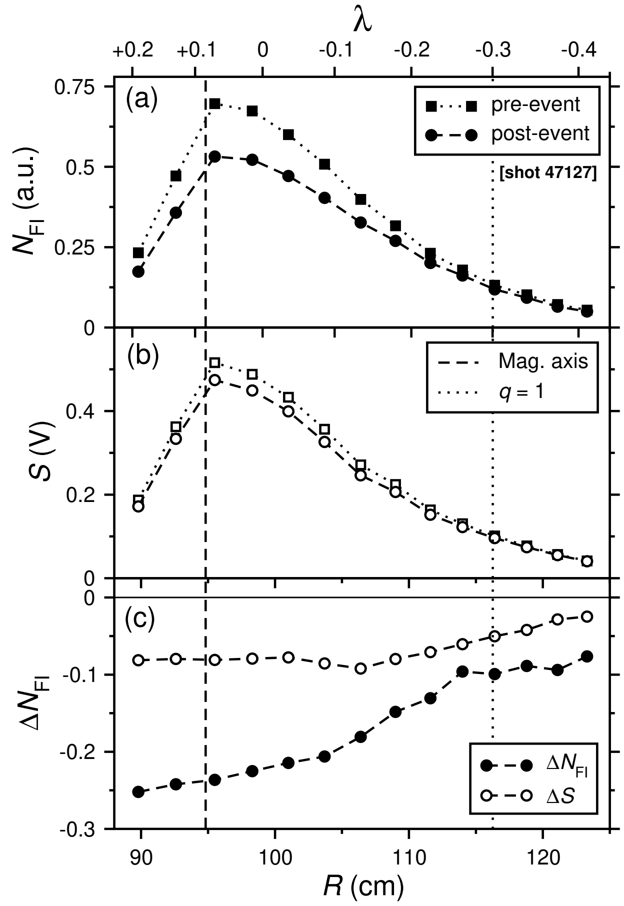

FIG. 7: Comparison of fast-ion population densities, $N_{\rm FI}$ (a), and total ssNPA signals, S (b), measured preceding and following a sawtooth event (t = 387 ms) identified in MAST-U shot 47127, shown as a function of major axis, R, and pitch, λ. Panel (c) gives the proportional changes in the respective quantities following the event. The positions of the magnetic axis and q = 1 surface along R are also indicated.

are directly measured using beam-emission spectroscopy to compare with those of the active signal. This would provide a measurement of the beam attenuation as well as a more accurate representation of the neutral-density oscillations at a given position along the beam line.

A method has been developed to determine the fast-ion population density, $N_{\rm FI}$, in magnetically-confined plasmas along a slice of the major axis, R, pitch, λ, variable space using ssNPA-signal, S, and NBI power-output, $P_{\rm NBI}$, data. Amplitudes of oscillations in the active-CX inducing NBI power output are compared with those reproduced in S, allowing for the active signal component to be separated from those of the passive and background;

the active signal being indicative of the $N_{\mathrm{FI}}(R, \lambda)$. This method allows for N_{FI} to be measured throughout NBI-heating and is therefore particularly useful for measuring changes in fast-ion populations following plasma instabilities. The method uses oscillations in S and P_{NBI} signal over small ranges to determine N_{FI}. This significantly mitigates issues related to detector non-linearity and off-sets in signal measurements compared with conventional techniques.

The authors would like to acknowledge D. Liu and M. Cecconello for his contributions to the manuscript. This work has been carried out within the framework of the EUROfusion Consortium, funded by the European Union via the Euratom Research and Training Programme (Grant Agreement No 101052200—EUROfusion). Views and opinions expressed are however those of the author(s) only and do not necessarily reflect those of the European Union or the European Commission. Neither the European Union nor the European Commission can be held responsible for them. This work has also been funded by the EPSRC (Grant No EP/T012250/1), the EPSRC Energy Programme (Grant No EP/W006839/1) and the US DoE (Grant No. DE-SC0019253). To obtain further information on the data and models underlying this paper please contact PublicationsManager@ukaea.uk.

---

[1] K. Shinohara, D. S. Darrow, A. L. Roquemore, S. S. Medley and F. E. Cecil Rev. Sci. Instrum. **75**, 3640 (2004).

[2] D. Liu, W. W. Heidbrink, D. S. Darrow, A. L. Roquemore, S. S. Medley and K. Shinohara Rev. Sci. Instrum. **77**, 10F113 (2006).

[3] Y. B. Zhu, A. Bortolon, W. W. Heidbrink, S. L. Celle and A. L. Roquemore Rev. Sci. Instrum. **83**, 10D304 (2012).

[4] D. Liu, W. W. Heidbrink, K. Tritz, Y. B. Zhu, A. L. Roquemore and S. S. Medley Rev. Sci. Instrum. **85**, 11E105 (2014).

[5] P. A. Schneider, H. Blank, B. Geiger, K. Mank, S. Martinov, F. Ryter, M. Weiland, A. Weller and the ASDEX Upgrade Team Rev. Sci. Instrum. **86**, 073508 (2015).

[6] D. Liu, W. W. Heidbrink, K. Tritz, E. D. Fredrickson, G. Z. Hao and Y. B. Zhu Rev. Sci. Instrum. **87**, 11D803 (2016).

[7] G. Prechel, N. Fil, D. Liu, W. W. Heidbrink, C. Michael, A. R. Jackson and MAST-U Team

Rev. Sci. Instrum. **93**, 113517 (2022).

[8] W. W. Heidbrink Rev. Sci. Instrum. **81**, 10D727 (2010).

[9] C. Vincent, S. Allan, G. Naylor, R. Stephen, S. Bray, A. Thornton and A. Kirk Rev. Sci. Instrum. **93**, 093509 (2022).

[10] M. Cecconello, M. Turnyanskiy, S. Conroy, G. Ericsson, E. Ronchi, S. Sangaroon, R. Akers, I. Fitzgerald, A. Cullen and M. Weiszflog Rev. Sci. Instrum. **81**, 10D315 (2010).

[11] J. F. Ziegler, M. D. Ziegler and J. P. Biersack Nucl. Instrum. Meth. B **268**, 1818 (2010).

[12] D. Liu, W. W. Heidbrink, M. Podestà, G. Z. Hao, D. S. Darrow, E. D. Fredrickson and D. Kim Nucl. Fusion **58**, 082028 (2018).